Stereology of Dimple Fracture and Mechanical Properties Correlations in an Austenitic Alloy With Few Inclusions

Oswaldo A. Hilders[1]; Daniel Pilo[2]; Mitsuo Ogura[3] and Andrés E. Mora[4]

1 Escuela de Ingeniería Metalúrgica y Ciencias de los Materiales. Universidad Central de Venezuela. Apartado 51717, Caracas, 1050-A, Venezuela. 2 Departamento de Ingeniería Mecánica. Universidad Simón Bolívar. Caracas, Venezuela. 3 Centro de Microscopía Electrónica. Facultad de Ciencias Universidad Central de Venezuela. Caracas, Venezuela. 4 Centro de Microscopía Electrónica. Facultad de Ciencias. Universidad de los Andes. La Hechicera. Mérida, Venezuela.

ABSTRACT

The effects of temperature and time of aging on ductile fracture, were investigated in an austenitic stainless steel with few inclusions. From cylindrical tensile data and stereological correlations, a mechanism of void formation is proposed. Two stages can be envisaged for the mechanism of voiding: (1) an homogeneous nucleation process is aided by the vacancies generated by dislocation interaction. (2) a limited vacancy-cluster coalescence process can be developed, from the excess vacancies preserved by quench, which annihilate at the voids leading to the growing of them. Longer or increased times and higher temperatures produced smaller dimple sizes, being this effect acompanied by the progresive reduction in yield strength and an increased values of ductility and surface relief.

KEYWORDS

Dimple fracture, void nucleation, stainless steel, fracture profile, ductile fracture, vacancy, fracture roughness.

INTRODUCTION

Fracture of materials is broadly classified into ductile and brittle. In the case of materials containing second phase particles, it has been demonstrated that voids are nucleated at these particles. During further deformation, the voids enlarge and coalesce eventually resulting in dimpled fracture. The mechanism by which void nucleation occurs is either, by the fracture of particles, or by the particle/matrix interfase decohesion. Dislocation bowing between particles leaves dislocation loops around them, which will separate the particles from the matrix [10]. dislocations also either climb over the particle by forming jogs, or pile up at the particle, resulting in fracture of particles [21]. In general, the nuclei for ductile fracture, in nominally single-phase materials, are inclusions or precipitate particles.

In some alloys, a significant inclusion population is rarely present, and fracture surfaces only ocassionally reveal particles within ductile dimples. In two phase alloys, there is evidence that dimples can be nucleated at interphase interfaces[22,31,42]. On the other hand, for singlephase alloys, even though several dislocation mechanisms for ductile fracture have been proposed, there is not yet a clear indication of the nucleation process for the case of particle-free dimples. While cavity initiation sites within grains are generally associated with hard second phase particles or nonmetallic inclusions, there has been evidence to indicate that under certain conditions, voiding can occur homogeneously. Bauer et al [4] have observed the openin up of cavities in front of propagating cracks in high purity single crystal silver foils. A similar process was observed in polycrystaline stainless steel, with some cavities opening up in particle free regions. Nevertheless, many cavities were formed in areas characterized by high dislocation densities. In such regions, the material has exhausted its ability to work harden and with the

triaxial stresses at he crack tip, internal cracking occurs. The dislocations running into the cracks allowing them to open up into stable cavities. Bauer et[5] propose that vacancies, produced in the regions of high dislocation density, condense to form voids. However, Balluffi and Seigle [2] have shown that unless there exist cavity nuclei of reasonable size within a grain, the excess vacancy concentration generated during deformation, probably never reaches a high enough value to form cavities homogeneously.

The vacancy-based theories for void nucleation are not yet disproved and they can be useful to explain the relationships between the fracture morphology and the mechanical properties in systems where no evidence of nucleating precipitates and inclusions are found. The need for a quantitative study of the relationships of dimpled fracture surfaces to mechanical properties is due to the fact that the ductile dimple rupture is common to a wide variety of metals or alloys of all strength levels, showing a important changes in strength, ductility and toughness [3,6,7,9,26]. Particulary, for austenitic stainless steels, which are the major structural meterial for currently operating and planned fast breeder reactors all over the world[19], the failure during any forming operation is invariably due to ductile fracture. There is evidence that the reduction in area, RA, due to changes in some experimental conditions [39] (like introduction of hydrogen) is strongly correlated with the reduction in microvoid fracture surface dimple size, being the RA loss for 304L type stainless steel, nearly 60% for a corresponding 70% reduction in dimple size. On the other hand, neutron irradiated type 321 stainless steel exhibed a significant reduction in fracture toughness together with a dramatic refinement in the scale of microvoid coalescence [34].

Although stainless steels have existed throughout the major part of this century, the development rate continues to increase. They are important in connection to our environment and safety, to an increasingly advanced industry and to the improved understanding of the importance of the total cost of a structure during its economic life. The present paper describes the results of a detailed investigation on the effects of heat treatments (aging) between 550°C and 850°C, on some mechanical properties, dimple characteristics and fracture topography of a commercial austenitic alloy AISI 304. For a low density of paticles or inclusions associated to dimples over the fracture surface, the vacancy origin of voids could be important in alloys thermal aged and quenched.

EXPERIMENTAL PROCEDURE

Material

The material used in this study was a commercial 304 type stainless steel received in the form of a rolled bar previously solution annealed at 1050°C during 1 hour, and quenched in water at room temperature. The chemical compostion of the alloy (in weigth percent) is: 17.89 Cr; 9.69 Ni; 0.070 C; 1.45 Mn; 0.35Si; 0.022 S; 0.020 P; 0.20 Mo and 0.09 Cu.

Specimen Preparation and Testing

Smooth axysimmetric tensile specimens were machined with a 2.54-cm gage length and a 0.635-cm gage diameter, in accordance with the ASTM standards[1]. The specimens were heated for 1, 2, 3 and 5 days at each of the following temperatures: 550°C, 700°C and 850°C.

Tensile tests were conducted to fracture at room temperature, on a floor model Instron at a constant crosshead speed of 4.2×10^{-4} cm/sec. The true stress and true plastic strains before necking were calculated from the load-time chart recordings assuming constant volume conditions, and the post-uniform strains, from the difference between the total and uniform strains.

Microscopy

After tensile testing, the fracture surfaces of the specimens were cleaned and examined under a HITACHI S-500 scanning electron microscope (SEM) operating in the secondary electron image mode at 25 Kv. In addition, in order to determine the nature of the fracture surface, fractured tensile halves were sectioned longitudinally, mounted in plastic, polished and etched. Metallographic studies were performed on these sections, for each time-temperature experimental conditions.

Dimple Stereology and Fracture Path

SEM obsservations on the fracture surface were conducted to determine the size of the dimples, which is taken in this study as the apparent mean radius of the circle, $\bar{b}'$, obtained by the intersection of the ellipsoid of revolution which constitutes a void, with the fracture surface [12,26]. A statistical distribution of dimple sizes was obtained by determining a

number of concentric fracture surface areas, just at the center portion of the fractured samples, and measuring the void diameters inside each one, using a line intercept method. The fractographs over which the measurements were made, have been taken paralell to the mean plane of fracture. The fracture surface areas were defined by using the Mandelbrot-Richardson's method [11], delineated in Fig. 1-a. Zones 1, 2 and 3 show several situations for a void or a couple of voids on the frontier of the broken line (point 4) which defines a closed area. Figures 1-b, 1-c and 1-d, are examples of the area contours obtained for different experimental conditions, which will be explained latter. The number on each contour, represents the number of voids inside the corresponding area.

The areal density of cavities beneath the fracture surface, NA, determined on longitudinal sections of the tensile specimens, was studied as a function of the axial distance from the fracture surface, Z. Since fracture takes place on the minimum section of the neck (radius a), This method has been already used by several authors [14, 17, 18].

Following the measurements of the areal density of cavities, the fracture profiles were studied using an OMNIMET-image analyser to determine the profile roughness parameter, Rℓ[13,40] defined as the ratio of the true length of the fracture line to its projected length on a reference line.

RESULTS

Dimpled Topography

A detailed examination of the fracture surfaces and longitudinal polished sections, showed different fracture morphologies, depending on the aging temperature and the holding time. Nevertheless, at any aging temperature, the fracture surfaces of the aged material for different times were very similar to one another. In general, the fracture surfaces of the tensile specimens are of the cup-and-cone type, but wich showed radial intergranular secondary cracking developed extensively all over the surface.

At 550°C and 700°C, the fracture morphology consisted of ductile dimples, as shown in Fig. 2, (1 day at 550°C). It can be observed the fracture path which encompass the entire fracture profile (Fig. 2-a). For axysimmetric tensile specimens which fail by void coalescence and exhibit a cup-cone fracture mode, failure initiates at the center in the necked region [8,36]. Here, the deformation mode is axysimmetric with no shear stress acting on the region, leading to an almost equiaxed dimples (Figures 2-c and 2-d). This coalescence mode has been referred to as normal rupture [6,38]. The particular morphology delineated for the fracture profile, indicates that the shear lip region in the left side is unusually large, leading to a shear rupture process in which the coalescence occurs under the combined influence of plastic strain in the direction of the applied stress and shear strain on a plane of maximum shear stress. The resulting fracture morphology is that of an elongated or parabolic dimples (Figure 2-b). On the other hand, the shear lip zone at the right side, is very small, and the dimples in the corresponding fracture surface are less elongated, (Figure 2-d), since the shape of the shear dimples depends upon the local ratio of normal strain to shear strain, which is smaller than in the opposite shear lip.

The Fig. 3 shows a close insight into this two mechanisms. It can be seen that the large and elongated shear dimples displayed on the fracture surface of Fig. 3-a, differ markedly from the normal dimples on the fracture surface of Fig. 3-b. Normal dimples appeared to be deeper than the shear dimples. An important observation is that there is no significant difference in the fracture topography of the samples aged at 550°C and 700°C. In the latter figure, two characteristics dimples, 1 and 2, are pointed by arrows.

Mixed Rupture

SEM observations on the fracture surface of the samples aged at 850°C, revealed a mixture of dimples and intergranular morphology, with no evidence that the failure had originated at a pre-existing defect. Further observations on longitudinal as-polished sections of these samples, revealed secondary cracking processes, with cracks lying parallel to the stress axis. Although intergranular fracture was observed, the proportion of dimpled fracture was considerably higher than intergranular fracture. Fig. 4 depicts an example of a specimen aged for one day at 850°C. In (a) [27], on point 1, a local severe intergranular separation can be observed, Point 2 shows a large shear facet, which is further detailed at (b). A very fine micro-dimple structure and an incipient secondary cracking is observed in the later figure. Points 3, 4, 5, 6 and 7, on (a), show a small shear facets. Another view of the intergranular cracking is observed on (c).

Fig. 4-d is a higher magnification view of region 1 in (c), showing some facets numbered 1, 2, 3 and 4, which were estimated to be aobut one half the size of the grains. Figure 5 is an example of the microstructure associated to a step-wise cracking behaviour.

Cavity Distribution and Dimple Size Distribution Analysis

Figure 6 shows the areal density of cavities as a function of the parameter Z/a_o. This quantitative metallography was accomplished at a magnification of 1000 times. The curves representing the distribution of areal density of cavities, correspond to 1 day of aging at the three different temperatures. No significant differences on the tendency of the curves were observed for other times of heat treatment. The relative position of the curves will be discussed in terms of the relationship between the density of the cavities, the role played for the vacancies and the possible influence of the carbide precipitation distribution.

The statistical analysis of the size distribution of dimples is shown in Fig. 7. Two dominant features are important in this distribution: The longer the holding time at each temperature, the smaller the dimple size, and the higher the aging temperature, for a constant holding time, the smaller the dimple size.

The fracture surface area covered for each dimple size determination, (i. e. for eac time-temperature condition) was about 500 μm^2, in one mounted fractograph. Two mounted series of fractographs were used in each case. The shadow portion of some colums of the histogram in Figure 7, corresponds to the increment in frequency detected when the total area of analysis was larger, i. e. by analyzing three or four mounted fractographs. Although some conditions remain unchanged, for the altered distributions, just the maximum variation is reported, which in turn, coincides with the highest frequency column. In other words, there is no significant changes in the reported trends of $\bar{b}'$, since the relative position of its value for each distribution (broken lines) remain in the same column. Only the conditions for 1 and 3 days at 850°C could be moved at low values of $\bar{b}'$, but the general trend is unchanged.

Fracture Surface Profilometry

The surface relief of the fracture surfaces, and its correlations with the mechanical properties, were developed from the concept of profile roughness parameter $R\ell$. A theoretical relationship between $R\ell$ and Rs, (The surface roughness parameter) can be used to account for R from experimental values of Rs[16]:

$$\frac{1}{R} = \frac{4}{\pi} \sum_{n=0}^{\infty} \frac{(-1)^n (2-Rs)^n}{(2n+1)(Rs)^{n+1}} = \frac{4}{\pi} \left[\frac{1}{Rs} - \frac{2-Rs}{3Rs^2} + \frac{(2-Rs)^2}{5Rs^3} - \cdots \right] \quad (1)$$

where the first term represents the randomness of the fracture surface, and the higher order terms, the displacements from the perfectly random fracture surface. Although Underwood [41] has considered that the parameter Rs is the most important in quantitative fractography, however, some results [37,43] have shown that experimental values of Rs are not sensitive to important changes in fracture behaviour [16]. In addition, Rs is relatively inaccesible, which limitates the usefulness of equation 1. R values were obtained assuming that the fracture surface does not contain overlaps. In this case, a plane normal to the mean fracture plane, defines a line of length L which may be related to its projection L' on the mean fracture plane by the relation:

$$L = R\ell L' \quad (2)$$

This simple length ratio will be used as indicator of changes in fracture micromechanisms, and can increase either by a more tortuous curve or by higher peaks.

DISCUSSION

Mechanical Properties

A summary of the tensile test data at room termperature are given in Table I. It can be seen that the time and temperature of aging have little or no effect on the strength parameters. Nevertheless, at 700°C, after 5 days of aging, the tensile strength and the fracture strength increase. It can be explained in terms of the higher work-hardening rate observed for this condition, which in turn is a consequence of the lowering in the staking fault energy because of the continuous reduction fo the pct C in the Cr depleted zones [25], as the aging progresses. On the other hand, the yield strength, in the same condition, shows the smallest value, which would be difficult to explain, since after 120 hours of heating, an appreciable amount of precipitation of carbides of the type $(CrFe)_{23}C_6$, has been taking place, especially at grain boundaries. The resulting yielding can be a consequence of the balanced contributions of the differentially stressed zones of the material, i. e. the carbon-chromium depleted (sensitized) austenite, and the rest of the γ phase.

Since there is an optimum alloy content for the maximum total strain at fracture [35], the effect of the chemical changes during the aging process can affect this parameter. In other words, the $(CrFe)_{23}C_6$ precipitate, which impoverishes the matrix, is deleterious to ductility, as can be seen from the fracture strain and reduction in area data, for 550°C; but chemical changes can be associated to long times of aging, particularly at temperature as high as 700 and 850°C, where the dissolution of carbides takes place. This later effect has been observed by others investigators [32,33] during the elevated temperature aging of austenitic stainless steel base alloy. Table I shows the related increase in ductility associated to the higher times of aging at the higher temperatures.

Dimple Size and the roll of Vacancies

Cracked surfaces of the samples aged at 850°C have dimples smaller than those from total dimple fracture. The aging effect on the dimple size is displayed in Fig. 8. This shows a plot between dimple size values obtained for specimens aged at 550°C, 700°C and 850°C, vs yield strength (Rp) and time of aging. In addtion, this figure shows the relationship between the true fracture strain and the dimple size. In general, higher times and temperatures, produced smaller dimple sizes, being this effect acompanied by the progresive reduction in Rp and an increased values of ductility. The only exception of this behaviour, is the corresponding to the 550°C, which shows a little variation in Rp vs $b^{'}$, and direct linear relationship between ε_f and b^1. Then, smaller yield strength and higher ductilities associated with smaller dimples sizes for both, 700 and 850°C, could be related to the conditions of previous precipitation at those temperatures, and to the nature of the nucleation of voids.

Since very rarely was there any indication of a precipitate nor an inclusion within a dimple, alternate types of void nuclei should be considered, for example, vacancy clusters. Voids in this case are thus expected to nucleate and/or grow by a mechanism which is basically different to those suggested to occur in materials containing second-phase particles, i. e., void nucleation by interface decohesion or fracture of particles [23].

The coarser dimples dominant in the material aged at 550°C, can be attributed to the particle (carbides) distribution. At this temperature, the size of the carbides were roughly the same than that for 700°C or 850°C although the interparticle spacing was larger, which, in turn, leaves a larger space to the growth of the voids. Then, the size of the voids can not be attributed to the contribution of quenched vacancies, since the corresponding equilibrium concentrations are $C_v^{550} \cong 8 \times 10^{-7}$, $C_v^{700} \cong 7 \times 10^{-6}$, and $C_v^{850} \cong 3.4 \times 10^{-5}$, (an estimated values, taking $E^f_v \cong 1$ eV) [20] which differ in just one or two orders of magnitude. The void nucleation process is aided by the vacancies generated by the dislocation interaction. The voids grow more rapidly in the material aged at 550°C, since they nucleated homogeneously and a limited vacancy-cluster coalescence process would be developed more easily, as the free path between the precipitate carbides is larger, leaving the excess vacancies preserved by the quench, annihilate at the voids already nucleated.

The homogeneous nucleation process of ductile cavities in this type of material, has been observed already [28,29], but the role played by the vacancy clusters could only be significant in the early stages of nucleation and growth. At the final stage of growth and coalescence, the process is expected to be controlled by the dislocations. The density of the cavities, as an indirect evidence for the corresponding sizes, can be directly analyzed on the fracture surface. As was

shown in figures 1-b, 1-c and 1-d; (aged 5 days at 850°C, 2 days at 700°C and 1 day at 550°C respectively) the fracture surfaces are associated to a certain "density lines", which indicates the number of cavities enclosed by each one. Void measurements were not confined just to the fracture surfaces, but to the longitudinal sections as was explained. Figure 6 demonstrates the influence of the relative depth below the fracture surface, on the density of cavities. It can be seen, that for any given value of depth, the higher the aging temperature, the higher the density of cavities. This simple means that the size of the voids on the fracture surface will be smaller as the aging temperature becomes higher. In other words, the relative density differences are the same for the voids below the fracture surface, even when they are not totally developed, i. e., they are in some intermediate stage of growth.

Mechanical Properties-Fracture Topography Relationship

The fracture topography is related to the microstructural changes that occur upon aging. The variations in ductility are accompanied by significant changes in fracture profilometry. Although the main fracture region appeared to be relatively similar for all the samples tested at room temperature (since the main part of the surfaces consisted of numerous ductile dimples) the path of crack propagation was generally different, in that the surface relief at the center of the cup portion of the fracture increases as the fracture strain increases. This behaviour is accompanied by a derease in the dimple size, which is demonstrated in the Fig. 9.

It is evident that the geometric attributes of fracture surfaces, such as R_ℓ , and the associated microstructural features ($\bar{b}'$ for example) main contain quantitative information concerning the processes that lead to fracture. For an "homogeneous" nucleation of voids, the problem to relate the true strain at fracture, to R_ℓ or $\bar{b}'$, is very difficult, since there is not a population of particles which act as nuclei. In general, an increase in the effective volume fraction of particles, lead to a decrease in true strain at fracture [15,30], accompanied by a reduction in microvoid fracture surface dimple size.

There is a direct relationship between R_ℓ and ε_f, since the more deformation energy stored, the higher the fracture surface relief. In other words, ductile crack propagation required more energy, and the resulting separated surfaces reflected a rougher pattern, because of the plastic relaxation process. On the other hand, there is an inverse relationship between $R_\ell$and $\bar{b}'$, which arises from the consideration of the growth of voids. If the voids grow primarily in the direction of the tensile stress, we can expect an enlargement of the major axis of the ellipsoid of revolution which constitutes a void, as the ductility of the material increases, and an increase in the depth-to-width ratio of the dimples in (absence of any inclusion, i. e., for "homogeneous" nucleation). Thus, since $\bar{b}'$ is defined as the half of the diameter of the circle made by the intersection of a void with the main plane of fracture [24], it is expected a decrease in $\bar{b}'$ as the values of ε_f and R_ℓ increase. It is interesting to note, that there were not a loss in ductility for the samples aged at 850°C. Furthermore, in general, the higher ductilities were related with those samples. The local losses in ductility originated in the intergranular separation, are counterbalanced by the higher deformation capacity of the austenite matrix. Figure 10 shows a pair of fractographs corresponding to the aged conditions of 1 day, (a) and 3 days (b) at 850°C. In (a), points 1, 2 and 3 show micro-dimple structures associated with intergranular cracking. Additionally, point 4 shows a micro-dimple structure on a grain which has been fractured transgranularly. In (b), it can be seen intergranular fracture facets, with evidence of slip traces (point 1, for example) suggesting that plastic deformation via dislocation gliding is accompanied by the intergranular fracture.

SUMMARY

A mechanism of void formation can be envisaged, in which the homogeneous nucleation is aided by the vacancies generated by dislocation interaction. Then, a limited vacancy-cluster coalescence process can be developed, leaving the excess vacancies preserved by the quench, annihilate at the voids, leading to the growing of them. Higher times and temperatures, produced smaller dimples sizes, being this effect acompanied by the progresive reduction in Rp and an increased values of ductility and surface relief.

ACKNOWLEDGEMENTS

This work was supported by the CDCH of the Central University of Venezuela (Nº 09.17.1787.86).

RESUMEN

Se investigó el efecto de la temperatura y el tiempo de envejecimiento, en la fractura dúctil de un acero inoxidable austenitico con pocas inclusiones. Se propone un mecanismo de formación de cavidades, basado en correlaciones estereológicas y resultados de ensayos de tracción. El mecanismo en cuestión, puede dividirse en dos etapas:
(1) El proceso de nucleación de cavidades es favorecido por las vacancias que se generan debido a la interacción de dislocaciones.
(2) Se desarrolla un proceso de coalescencia de las vacancias en exceso que han quedado atrapadas en la red después de un enfriamiento brusco, las cuales se aniquilan en las cavidades, provocando el crecimiento de las mismas. Largos períodos de permanencia a altas temperaturas, generan menores tamaños de cavidad. Este último efecto, está acompañado por la progresiva reducción del esfuerzo de fluencia y el aumento de la ductilidad y la rugosidad de las superficies de fractura.

Palabras clave: Fractura por coalescencia de cavidades, nucleación de cavidades, acero inoxidable, perfil de fractura, fractura dúctil, vacancia, rugosidad de la superficie de fractura.

REFERENCES

1. Annual Book of ASTM Standards. (1971). Round Tension Test Specimen, A 370, part 31, ASTM Philadelphia, Pa., pp. 4-54.

2. Ballufi, R. W., and Seigle, L. L. (1955). Effect of grain boundaries upon pore formation and dimensional changes during diffusion. Acta Met. 3: 170-177.

3. Bates, R. C. (1984). Modeling of ductile fracture by microvoid coalescence for the prediction of fracture toughness. In J. M. Well, R. E. Stolz and J. D. Landes (ed.), Fracture: Interactions of Microstructure, Mechanisms and Mechanics, pp. 117-155. AIME, Warrendale, Pa.

4. Bauer, R. W., Lyles Jr., R. L., and Wilsdorf, H. G. F. (1972). Die direkte untersuchung der riβbildung in metallen im hochspannungs elektronenmikroskop. Z. Metallk. 63: 525-530.

5. Bauer, R. W., and Wilsdorf, H. G. F. (1973). Void initation in ductile fracture. Scripta Met. 7: 1213-1220.

6. Beachem, C. D. (1963). An electron fractographic study of the influence of plastic strain conditions upon ductile rupture processes in metals. Trans. ASM 56: 318-326.

7. Beachem, C. D. (1975). The effects of crack tip plastic flow directions upon microscopic dimple shapes. Met. Trans. 6A: 377-383.

8. Becker, R., Smelser, R. E., Richmond, O., and Appleby, E. J. (1989). The effect of void shape on void growth and ductility in axisymmetric tension test. Met. Trans. 20A: 853-861.

9. Bray, J. W., Handerhan, K. J., Garrison Jr., W. M., and Thompson, A. W. (1992). Fracture toughness and the extents of primary void grwth. Met. Trans. 23A: 485-496.

10. Broek, D. (1974). Some contributions of electron fractography to the theory offracture. In. Met. Rev. 19: 135-182.

11. Chermant, J. L., and Coster, M. (1978). L'objet fractal en analyse d' images. Proc. international Symposium on Quantitative Metallography, pp. 125-136. E. Ass. Italiana di Metallurgia, Florence.

12. Chermant, J. L., and Coster, M. (1979). Quantitative fractography. J. Mat. Sc. 14: 509-534.

13. Chermant, J. L., and Coster, M. (1989). Mathematical morphology and quantitative fractography. In K. Salama, K. Rawi-Chandar, D. M. R. Taplin and P. Rama-Rao (ed.), Advances in Fracture Research, pp 3373-3482. Pergamon. Oxford.

14. Cialone, h., and Asaro, R. J. (1981). Hudrogen assisted fracture of spheroidized plain carbon steels. Met. Trans. 12A: 1373-1387.

15. Cox, T. B., and Low, J. R. (1974). An investigation of the plastic fracture of AISI 4340 and 18 nickel-200 grade maraging steels. Met. Trans. 5: 1457-1470.

16. El-Soudani, S. M. (1978). Profilometric analysis of fractures. Metallography. 11: 247-336.

17. Fisher, J. R., and Gurland, J. (1981). Void nucleation in Spheroidized carbon steels. Met. Sc. 15: 185-202.

18. Garber, R., Bernstein, I. M., and Thompson, A. W. (1981). Hydrogen assisted ductile fracture of spheroidized carbon steels. Met. Trans. 12A: 225-234.

19. Gill, T. P. S., Vijayalakshmi, M., Rodríguez, P., and Padmanabhan, K. A. (1989). On microstructure-property correlation of termally aged type 316L stainless steel weld metal. Met. Trans. **20A**: 1115-1124.

20. Goldsmid, H. J. (1975). Problems in Solid State Physics. p. 241. Pion Limited, London.

21. Goods, S. H., and Brown, L. M. (1979). The nucleation of cavities by plastic deformation. Acta Met. **27**: 1-15.

22. Greenfield, M. A., and Margolin, H. (1972). The mechanism of void formation, void growth and tensile fracture in an alloy consisting of two ductile phases. Met. Trans. **3**: 2649-2659.

23. Hilders, O. A. (1981). Formación de vacidades a partir de inclusiones equiaxiales en la fractura dúctil. Acta Cient. Venez. **32**: 144-150.

24. Hilders, O. A. (1985). Fracture toughness determination for 304 austenitic stainless steel in terms of dimple size in tensile ductile fracture. Latin-Am. J. Met. and Mat. **5**: 97-104.

25. Hilders, O. A. (1992). Fracture path profilometric analysis, fracture toughness and mechanical properties in sensitized 304 stainless steel. In H. Nordberg and J. Björklund (ed.), Applications of Stainless Steels '92, **2**: pp. 1017-1027. Jernkontoret, Stockholm.

26. Hilders, O. A., and Santana, M. G. (1988). Toughness and fractography of austenitic type 304 stainless steel with sensitization treatments at 973 K. Metallography. **21**: 151-164.

27. Hilders, O. A., and Pilo, D. (1992). On the relationship between fracture toughness and fracture surface characteristics, an alternative criterion for predicting K_{IC} in ductile alloys. Proc. 2nd. International Congress on Energy, Environment and Technological Innovation **2**: pp. 357-362. Rome.

28. Hilders, O. A., and Pilo, (1992). Fractographic study of a sensitized AISI 304 type austenitic stainless steel. Acta Microsc. **1**: 52-57.

29. Hilders, O. A., Pilo, D., Ogura, M., and Mora, A. E. (1992). Fracture surface source of toughness in sensitized austenitic stainless steel. Proc. 1st. Atlantic Congress of Electron Microscopy, pp. 360-361. Mérida.

30. Knott, J. F. (1973). Fundamentals of Fracture Mechanics. Chap. 8 Butterworths, London.

31. Krishna Mohan Rao, Y., Kutumbarao, V. V., and Rama Rao, P. (1989). Influence of microstructure on void nucleation and growth in a near-α titanium alloy IMI 685. Mat. S. and Eng. **A110**: 193-202.

32. Lai, J. K. L., Chastell, D. J., and Flewitt, P. E. J. (1981). Precipitate phases in type 316 austenitic stainless stel resulting from long-term high temperature service. Mat. Sc. and Eng. **49**: 19-29.

33. Lai, J. K. L. (1983). A study of precipitation in AISI type 316 stainless steel. Mat. Sc. and Eng. **58**: 195-209.

34. Little, E. A. (1986). Fracture mechanics evaluations of neutron irradiated type 321 austenitic steel. J. Nucl. Mater. **139**: 261-276.

35. Pickering, F. B. (1976). Physical metallurgy of stainless steel developments. Int. Met. Rev. **21**: 227-268.

36. Rogers, H. C. (1960). The tensile fracture of ductile metals. Trans. AIME. **218**: 498-506.

37. Sigl, L. S., and Exner, E. E. (1987). Experimental study of the mechanics of fracture in WC-Co alloys. Met. Trans. **18A**: 1299-1308.

38. Speich, G. R. and Spitzig, W. A. (1982). Effect of volume fraction and shape of sulfide inclusions on through-thickness ductility and impact energy of high-strength 4340 palte steels. Met. Trans. **13A**: 2239-2257.

39. Thompson, A. W. (1983). The relation between changes in ductility and in ductile fracture topography: control by microvoid nucleation. Acta Met. **31**: 1517-1523.

40. Underwood, E. E., and Banerji, K. (1986). Fractals in fractography. Mat. Sc. and Eng. **80**: 1-14.

41. Undrewood, E. E. (1989). The current status of modern quantitative fractography. In K. Salama, K. Rawi-Chandar, D. M. R. Taplin and P. Rama-Rao (ed.), Advances in Fracture Research, pp. 3391-3411. Pergamon, Oxford.

42. Vijayaraghavan, T. V., and Margolin, H. (1988). The effect of matrix strength on void nucleation and growth in an alpha-beta titanium alloy, CORONA-5. Met. Trans. **19A**: 1321-1329.

43. Wanhill, R. J. H. (1988). Low stress intensity fatigue crack growth in 2024-T3 and T351. Eng. Fract. Mech. **30**: 233-237.

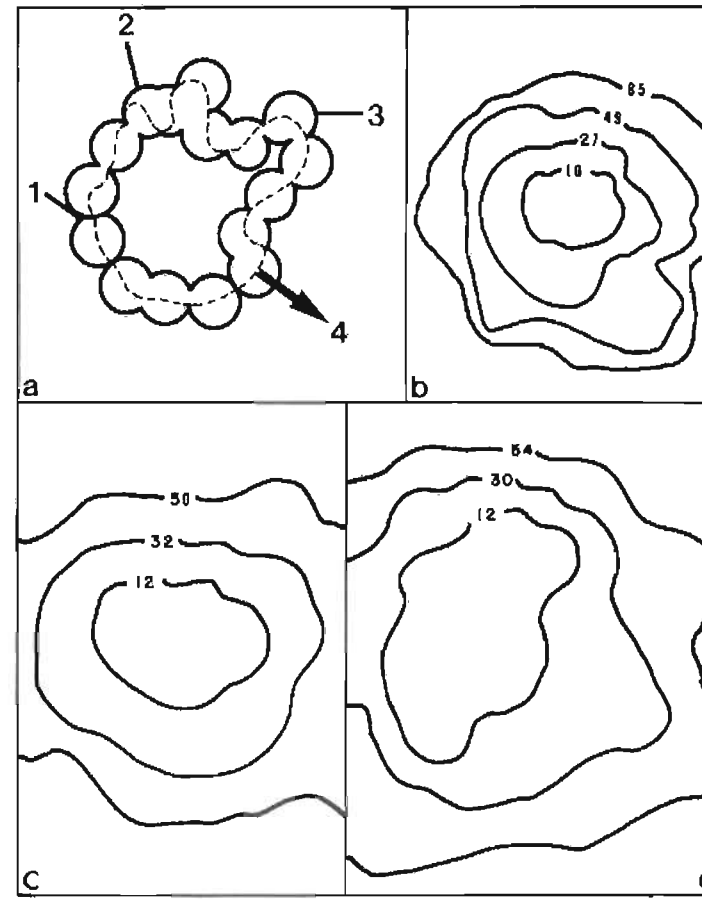

Fig.1

Fig. 1 (a) Schematic of the statistical distribution study of voids over the fracture surface. (b), (c) and (d): area contours at the center portion of the fractured samples, for aging times of 5, 2 and 1 day at 850, 700 and 550°C respectively.

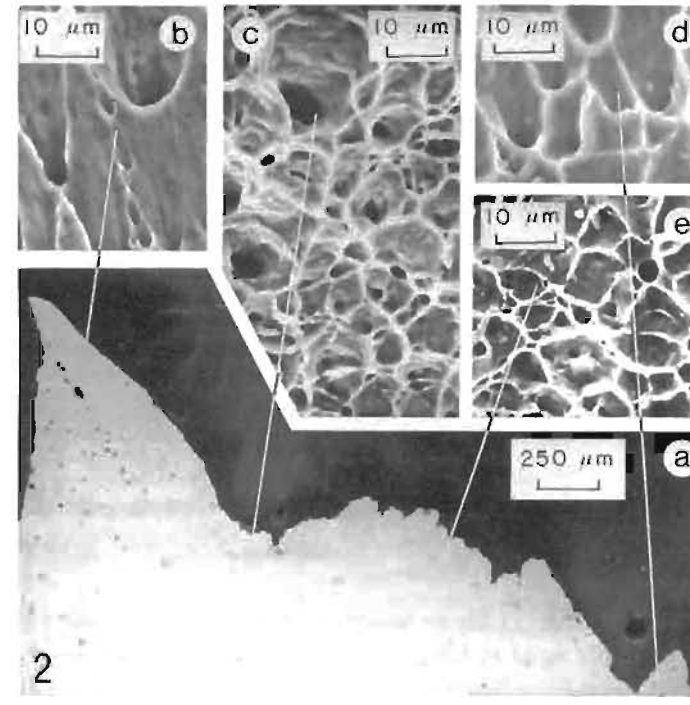

Fig. 2 Fracture profile and dimple morphology (SEM) associated with different zones over the fracture surface. (Sample aged at 550°C, for 1 day. For details see text).

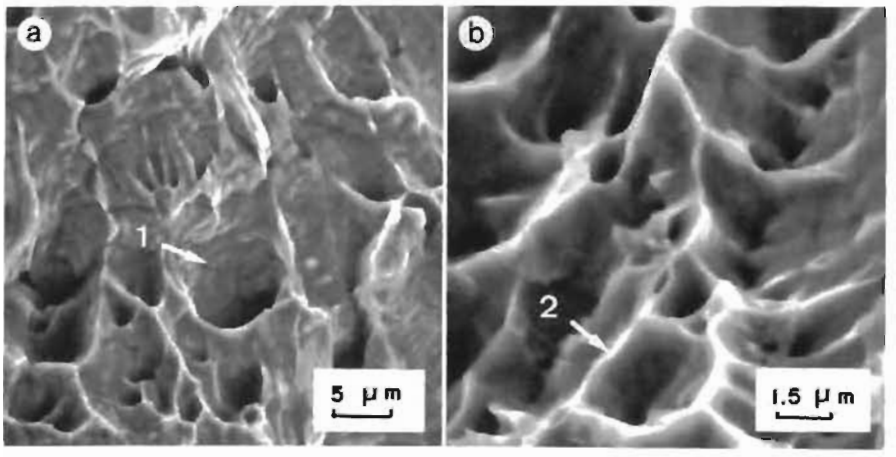

3

Fig. 3 Scanning electron micrographs, showing one basic mechanism of ductile rupture: microvoid coalescence, and two resulting dimple morphologies: (a) elongated shear dimples and (b) normal dimples. (Sample aged at 550°C for 1 day).

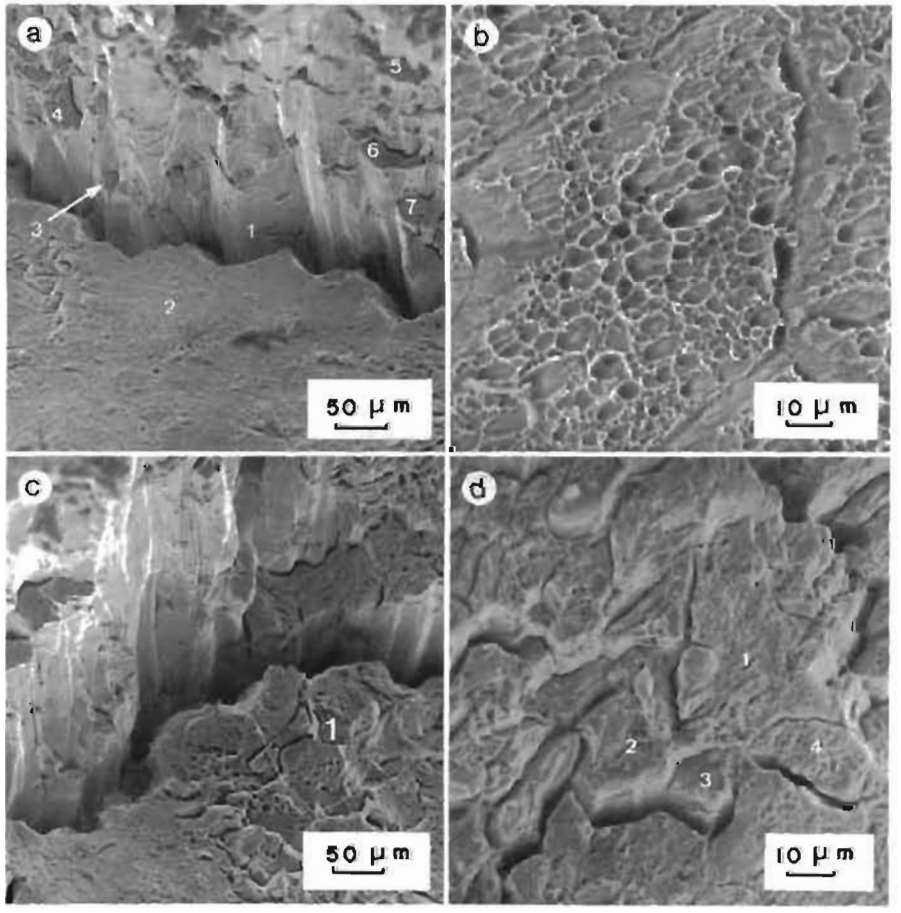

4

Fig. 4 Intergranular cracking process and mixed rupture mechanism (SEM) corresponding to the sample aged at 850°C for 1 day. (For details see text).

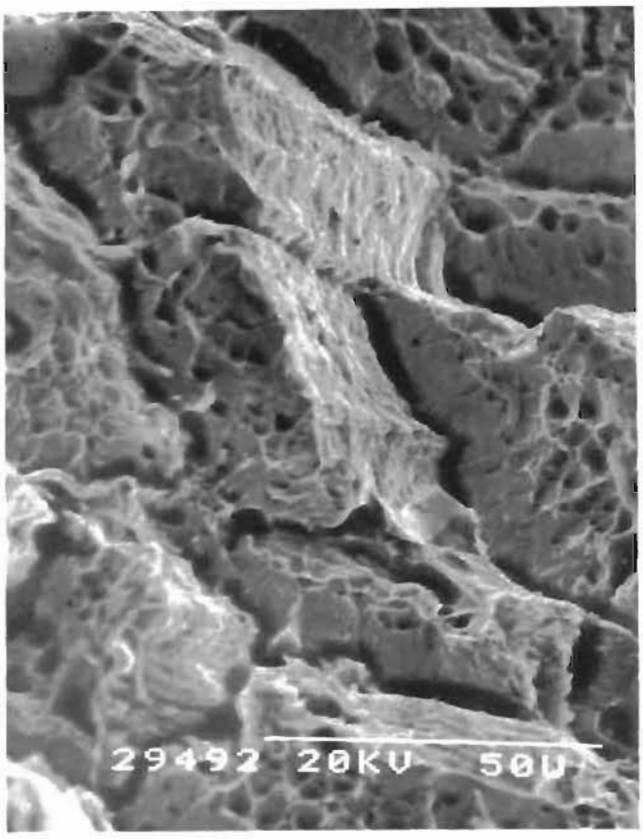

5

Fig. 5 Scanning electron micrographs for the sample aged at 850°C for 1 day, showing a step-wise cracking behavior.

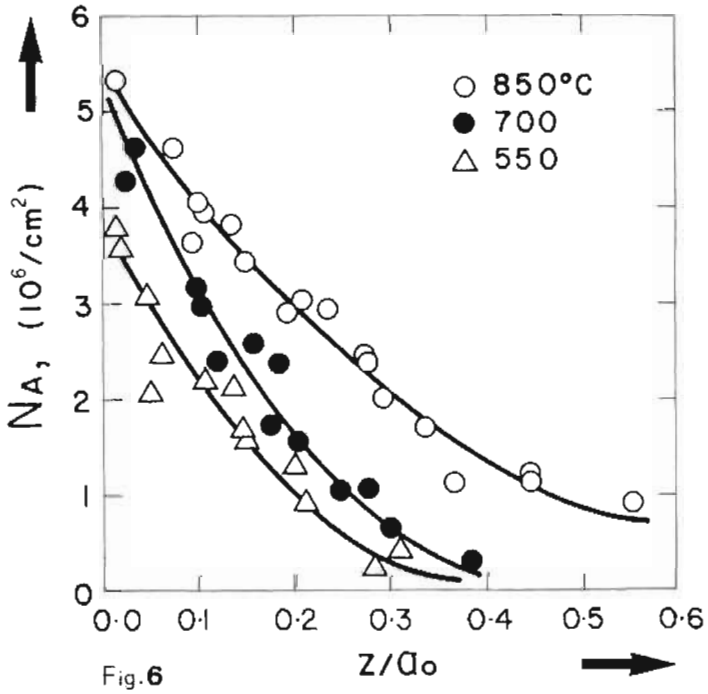

Fig. 6 Areal density of cavities as a function of the normalized axial distance from the fracture surface. The curves correspond to 1 day of aging at 550°C, 700°C and 850°C.

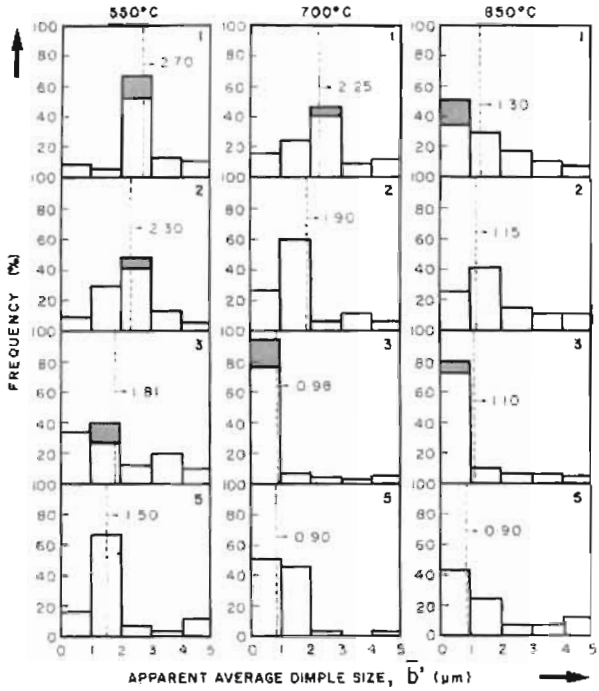

Fig.7

Fig. 7 Variation of void size distribution with temperature and time of aging (For details see text).

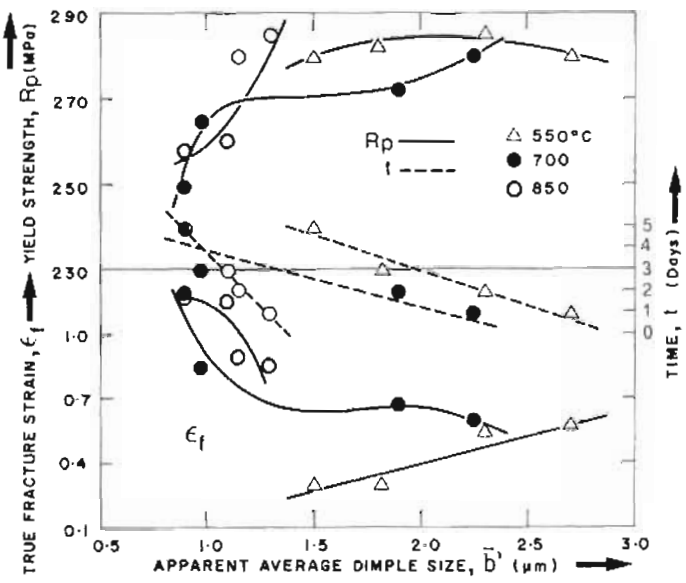

Fig.8

Fig. 8 Relationship between dimple size and yield strength, true fracture strain, time of aging and temperature of aging.

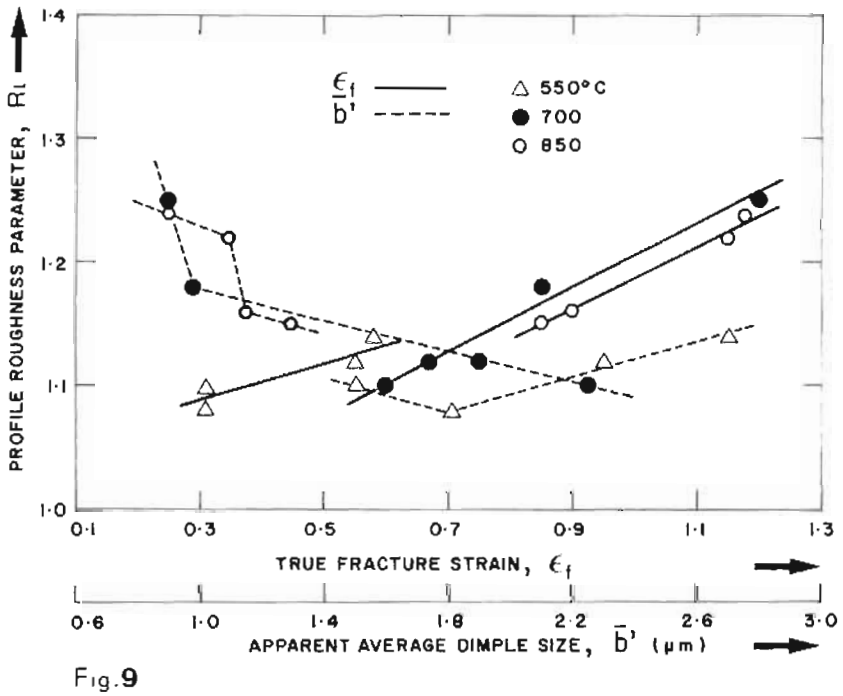

Fig.9

Fig. 9 Relationship between dimple size and true fracture strain, profile roughness and temperature of aging.

Table I: Tensile Test Data

Aging Temperature (°C)	Aging Tme (days)	Yield Strength (MPa)	Strength at Maximum Load (MPa)	Fracture Stress (MPa)	Strain to Maximum Load (pct)	Fracture Strain (pct)	Reduction in Area (pct)
550	1	280	581	691	42	58	44
	2	282	581	670	47	55	42
	3	285	581	691	27	31	27
	5	280	618	713	26	31	27
700	1	280	581	661	38	60	45
	2	272	581	701	56	67	49
	3	265	581	696	56	85	57
	5	250	618	728	65	120	70
850	1	285	581	691	53	85	57
	2	280	581	659	53	90	59
	3	260	581	701	53	115	68
	5	258	581	671	50	118	69

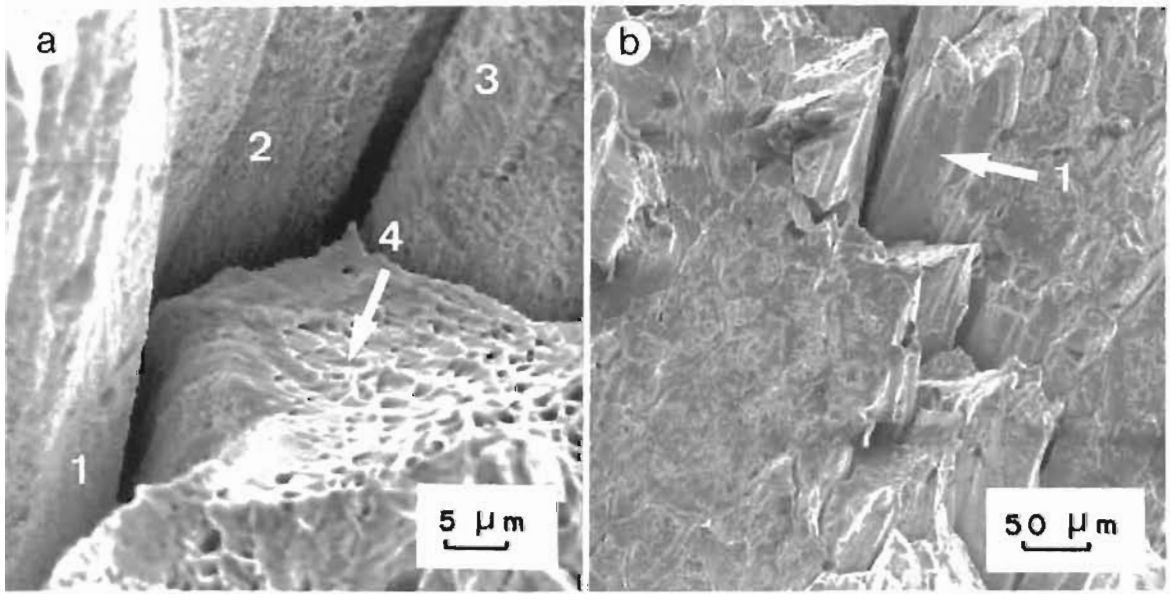

10

Fig. 10 Scanning electron micrographs showing some features of the mixed character of fracture for the samples aged at 850°C. (a) aged during 1 day, (b) aged during 3 days.